ELSEVIER

Chemical Engineering Journal 87 (2002) 367–379

Chemical Engineering Journal

www.elsevier.com/locate/cej

Consideration of numerical simulation parameters and heat transfer models for a molten carbonate fuel cell stack

Joon-Ho Koh*, Hai-Kung Seo, Young-Sung Yoo, Hee Chun Lim

Power Generation Laboratory, Korea Electric Power Research Institute, 103-16 Munji-dong, Yuseong-gu, Daejeon, 305-380 South Korea

Received 17 April 2001; accepted 16 October 2001

Abstract

A fuel cell stack model based on differential heat balance equations was solved numerically with a computational fluid dynamics code. Theoretical aspects in the simulation of a molten carbonate fuel cell (MCFC) performance model were discussed with regard to numerical accuracy of temperature prediction. The effect of grid setting for gas channel depth was studied to ensure how coarse it can be. A single computational element was sufficient for temperature prediction, while more grid elements are required for calculation of flow field and pressure distribution. The use of constant velocities is not recommended because it cannot account for the change of linear velocity within fuel cells, indicating the momentum equations have to be solved together with the heat balance equations. Thermal radiation has little effect on calculation of temperature field from the model. Gas properties vary within fuel cells, but most of them can be treated constant except for specific heat capacity of anode gas. Convection heat transfer by anode gas can be overestimated when a constant specific heat capacity is used, resulting in prediction of lower temperature curves. Overall, heat transfer in a co-flow stack is well characterized by two-dimensional model along the axial and vertical coordinates rather than on cell plane.

Keywords: Energy; Fuel cell; MCFC; Electrochemistry; Heat transfer; Numerical analysis

1. Introduction

Though its concept has been known for more than a century, commercialization efforts of fuel cell are just underway. Being an electrochemical energy conversion device, the major product of fuel cell is electrical power, but, it also produces a significant amount of heat. Heat management is one of the important problems in both low-temperature and high-temperature fuel cells. Fuel cell models can be built upon the conventional heat balance equations, but, further consideration of electrochemical reaction and its consequences should be taken into account at the same time. There have been many recent studies in this regard for the three most actively pursued fuel cell types: proton exchange membrane fuel cell (PEMFC), solid oxide fuel cell (SOFC), and molten carbonate fuel cell (MCFC).

Since a fuel cell stack is a pile of many cells, the stack model requires more equations and sometimes more complicated gas flow geometry than a single cell model. The purpose of a fuel cell stack performance model is to predict distribution of variables such as current density, temperature, and pressure. In fuel cell stacks, temperature can rise unexpectedly high due to the release of heat during cell reactions. Theoretical prediction of temperature distribution is important for stack design and stable operation, and it is achieved by solving a rigorous mathematical model. In our earlier work, we used an MCFC performance model to show the effect of stack operation variables such as cell length, stack height, feed gas temperature, stack heating temperature, current density, and gas utilization on temperature rise inside the stack [1]. In this paper, we will explore more fundamental characteristics in the numerical analysis of such a fuel cell stack model.

Usually fuel cell stack models require consideration of gas flow, heat transfer, mass transfer, and cell voltage–current relationship. In addition, the mathematical models need several thermal and flow parameters which are functions of temperature and gas composition. These transport parameters and model variables are mutually related, and they are in a wide range of modeling approach from the molecular level to the macroscopic level [2]. The complete solution algorithm is therefore a complicated iteration process. Simplification does help to get faster solution of fuel cell stack models. The consideration of gas flow may be simplified with constant velocities. It needs to be evaluated, however,

* Corresponding author. Tel.: +82-42-865-5393; fax: +82-42-865-5374.
E-mail address: koh@kepri.re.kr (J.-H. Koh).

1385-8947/02/$ – see front matter
PII: S1385-8947(01)00234-0

Nomenclature

A	surface or cross-section area (m^2)
C_p	specific heat capacity (J/mol K)
E_{eq}	equilibrium cell potential (V)
E^0	standard cell potential (V)
F	Faraday's constant (96487 C/equiv.)
h	heat transfer coefficient (W/m^2 K)
ΔH_f	enthalpy change of formation reaction (J/mol)
i	current density (mA/cm^2)
I	total current flow (A)
k	thermal conductivity (W/m K)
L	cell length (m)
m_{CO_3}	mass flux created or disappeared (kg/m^3 s)
M	molecular weight (g/mol)
N	molar flux (mol/m^2 s)
P_j	partial pressure of species j (atm)
q	rate of heat generation per unit surface area (W/m^2)
Q	volumetric rate of total heat generation (W/m^3)
Q_{cell}	rate of heat generation from fuel cell electrode reactions (W/m^2)
Q_{rad}	heat transfer rate by thermal radiation (W)
r_{H_2}	rate of hydrogen consumption by cell reaction (mol/m^2 s)
R	gas constant (8.314 J/mol K)
R_{ohm}	ohmic resistance ($\Omega\,m^2$)
T	temperature (K)
u_x	axial velocity (m/s)
u_y	vertical velocity (m/s)
V_{cell}	cell potential under electrical load (V)
x	axial coordinate (m)
y	vertical coordinate (m)
y_j	mole fraction of species j
z_j	stoichiometric coefficient of species j for cell reactions
Z	impedance for electrode polarization ($\Omega\,m^2$)

Greek letters

δ_g	gas channel depth (m)
ε	emissivity
θ	porosity
μ	viscosity (kg/m s)
ρ	density (kg/m^3)

whether the use of constant velocities guarantees a reliable computation result. The thermodynamic parameters may be considered constants. Since temperature and gas composition often varies significantly within fuel cells, however, it needs to be evaluated how those parameters are estimated and how they affect the accuracy of temperature prediction. These and more other issues will be explored in this paper. Specific attention was given for an MCFC stack where heat transfer characteristics is important to build and operate a commercial size stack. A two-dimensional model was considered to understand heat transfer in the main gas flow (axial) and stacking (vertical) directions. Specifically we investigated the effects of grid setting for gas channel depth, constant gas velocities, thermal radiation, and estimation of gas properties on prediction of temperature in MCFC. These are the issues that were not mentioned in the past fuel cell models and numerical simulation.

2. Mathematical model

2.1. General description of cells and stacks

The fuel cell stack model is described in Fig. 1. A cell is composed of electrolyte, anode, and cathode layers. The unit cell structure repeats with bipolar separator plates between them. Gas channels are created on both sides of the bipolar separator plates, being one for cathode gas and the other for anode gas. Many different fuel cells exist depending on which type of electrolyte is used. The overall fuel cell reaction is in most cases a formation of water from hydrogen and oxygen, producing electricity and heat.

$$H_2 + \tfrac{1}{2}O_2 \rightarrow H_2O + \text{Electricity} + \text{Heat} \quad (1)$$

Details of reaction mechanism are different from one type of fuel cell to another. MCFC utilizes a melted solution of carbonate salts (Li_2CO_3, K_2CO_3, and Na_2CO_3). Because these salts melt at above 500 °C, the operation of MCFC is done in the temperature range 600–680 °C where sufficient ionic conductivity is maintained. The following half-cell reactions take place in anode and cathode of MCFC. The electrolyte ions are conserved within the cell as they are consumed in the anode and generated in the cathode at equal amounts. The feed amount is determined by load current density (electricity to be withdrawn) and gas utilization (actual consumption of fuel and oxygen to their feed amounts).

$$H_2 + {CO_3}^{2-} \rightarrow CO_2 + H_2O + 2e^- \quad \text{(anode)} \quad (2)$$

$$CO_2 + \tfrac{1}{2}O_2 + 2e^- \rightarrow {CO_3}^{2-} \quad \text{(cathode)} \quad (3)$$

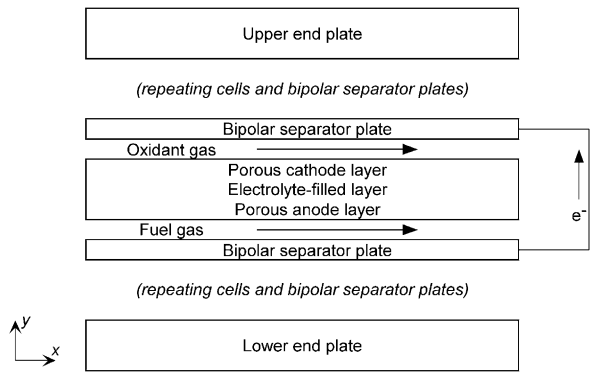

Fig. 1. Schematic diagram of the fuel cell stack model with a unit cell structure and co-flow separator plates.

The external reforming MCFC technology aims at the application in an integrated gasification fuel cell (IGFC) system. This application is expected only when a large-scale stack can be built with cell area near 1 m^2. There are many different types of stack design, and Fig. 1 depicts one of the typical MCFC stack models where both fuel and oxidant gas streams flow in parallel (called a co-flow configuration). The stack model in Fig. 1 is very simplified for a two-dimensional computation purpose, while the real stack has more complicated three-dimensional structure [1,3].

2.2. Relation between electrical power and thermal energy

The energy conversion efficiency of fuel cell is higher than that of combustion engines or boilers. Yet a significant amount of heat is released during the cell reaction. The amount of heat released is simply a subtraction of electrical energy from the enthalpy change of the overall cell reaction.

$$Q_{\text{cell}} = (-\Delta H_{\text{f,H}_2\text{O}}) r_{\text{H}_2} - iV_{\text{cell}} \tag{4}$$

where the enthalpy change is a function of temperature.

$$\Delta H_{\text{f,H}_2\text{O}} = -(240506 + 7.3835T)\ \text{J/mol} \tag{5}$$

The rate of fuel consumption is calculated from Faraday's law.

$$r_{\text{H}_2} = \frac{i}{z_{\text{H}_2} F} \tag{6}$$

where current density (i, mA/cm^2) varies from position to position and therefore the total current load is given by integration of local current density over the cell surface area. Though local current density is generally a function of space variables on the cell surface, the total current load (I) is given as an input variable for fuel cell operation.

$$I = \iint i\, \mathrm{d}A \tag{7}$$

The last term in Eq. (4) is electrical power from cell voltage under the total current load. This can be measured from experiments and also be calculated from potential balance.

$$V_{\text{cell}} = E_{\text{eq}} - i(R_{\text{ohm}} + Z_{\text{anode}} + Z_{\text{cathode}}) \tag{8}$$

where cell voltage is represented with equilibrium cell potential minus irreversible losses due to internal cell resistance and electrodes polarization resistance. Equilibrium cell potential is calculated from the Nernst equation.

$$E_{\text{eq}} = E^0 + \frac{RT}{2F} \ln \left[\frac{P_{\text{H}_2,\text{a}} \sqrt{P_{\text{O}_2,\text{c}}}}{P_{\text{H}_2\text{O,a}}} \frac{P_{\text{CO}_2,\text{c}}}{P_{\text{CO}_2,\text{a}}} \right] \tag{9}$$

$$E^0 = 1.2723 - 2.7645 \times 10^{-4} T \quad (\text{for reaction (1)}) \tag{10}$$

Internal cell resistance strongly depends on cell materials, contact resistance, and temperature. The following equation for internal cell resistance of MCFC was obtained from our experiments and literature [4].

$$R_{\text{ohm}} = 0.5 \times 10^{-4} \exp\left[3016 \left(\frac{1}{T} - \frac{1}{923} \right) \right] \tag{11}$$

The estimation of polarization resistance is not a thoroughly established part. There are some correlation equations available for MCFC [5].

$$Z_{\text{anode}} = 2.27 \times 10^{-9} \exp\left(\frac{6435}{T} \right) P_{\text{H}_2}^{-0.42} P_{\text{CO}_2}^{-0.17} P_{\text{H}_2\text{O}}^{-1.0} \tag{12}$$

$$Z_{\text{cathode}} = 7.505 \times 10^{-10} \exp\left(\frac{9298}{T} \right) P_{\text{O}_2}^{-0.43} P_{\text{CO}_2}^{-0.09} \tag{13}$$

2.3. Assumptions for simplification of the stack model

The equations needed for calculation of heat released during the MCFC operation are given above. As it shows, they are coupled by local current density, temperature, and partial pressure of gas species. It is usually assumed that the total system pressure is constant since pressure drop across cells is small (0.01–0.05 atm even for large-area cells) compared to the total pressure (1–15 atm). If we further assume a uniform local current density distribution, the calculation of cell voltage and heat release becomes much easier than solving for local current density by iteration. Then the relation for cell voltage and heat is a function of temperature and partial pressure.

Here, we will fix the total system pressure at atmospheric pressure, and then the partial pressure variables are reduced into gas composition variables. In the cell, some reactant gas species (H_2 in the anode and $0.5O_2 + CO_2$ in the cathode) have a decreasing concentration distribution from inlet to outlet. Concentration of product gas species ($CO_2 + H_2O$ in the anode) increases in the same direction. The variation of each gas concentration is a function of current density. Because we assume a uniform current density distribution, the cell reaction rate is considered uniform within the cell and is independent of local gas concentration. With this simplified cell reaction model, the gas composition is obtained as a function of one-dimensional space variable (axial distance) from a one-dimensional differential mass balance equation.

$$\frac{\mathrm{d}Ny_j}{\mathrm{d}x} = \frac{i}{z_j F} \frac{1}{\delta_{\text{g}}} \tag{14}$$

where N is a total molar flux and y_j's are gas mole fraction at a distance from the inlet (x). The right-hand side of Eq. (14) is the cell reaction rate which is constant for the uniform current density assumption, and δ_{g} is a gas channel depth. The gas composition for each species in MCFC anode with hydrogen as a primary fuel is then calculated from a set of given inlet composition.

$$y_{\text{H}_2} = \frac{1}{N_{\text{anode}}} \left(N_{\text{anode,in}}\, y_{\text{H}_2,\text{in}} - \frac{i}{2F\delta_{\text{g}}} x \right) \tag{15}$$

$$y_{CO_2(A)} = \frac{1}{N_{anode}}\left(N_{anode,in}\, y_{CO_2(A),in} + \frac{i}{2F\delta_g}x\right) \quad (16)$$

$$y_{CO} = \frac{1}{N_{anode}}(N_{anode,in}\, y_{CO,in}) \quad (17)$$

$$y_{H_2O} = \frac{1}{N_{anode}}\left(N_{anode,in}\, y_{H_2O,in} + \frac{i}{2F\delta_g}x\right) \quad (18)$$

The composition of MCFC cathode gases is obtained in the same way.

$$y_{O_2} = \frac{1}{N_{cathode}}\left(N_{cathode,in}\, y_{O_2,in} - \frac{i}{4F\delta_g}x\right) \quad (19)$$

$$y_{N_2} = \frac{1}{N_{cathode}}\left(N_{cathode,in}\, y_{N_2,in}\right) \quad (20)$$

$$y_{CO_2(C)} = \frac{1}{N_{cathode}}\left(N_{cathode,in}\, y_{CO_2(C),in} - \frac{i}{2F\delta_g}x\right) \quad (21)$$

where the total molar flow rates for anode and cathode are

$$N_{anode} = N_{anode,in} + \frac{1}{2}\frac{i}{F\delta_g}x \quad (22)$$

$$N_{cathode} = N_{cathode,in} - \frac{3}{4}\frac{i}{F\delta_g}x \quad (23)$$

Notice that CO in the anode is never involved in the cell reaction, but it exists in the anode gas mixture due to the following gas phase reaction. The amount of CO is calculated from chemical equilibrium conversion of a feed composition of H_2, CO_2, and H_2O. From the given feed composition shown in Table 1, it was known that approximately 10% of H_2 and CO_2 are converged into H_2O and CO. The gas composition profiles calculated from Eqs. (15)–(19) are plotted in Fig. 2, after taking into account this gas phase reaction.

$$CO + H_2O \leftrightarrow H_2 + CO_2 \quad (24)$$

2.4. Heat and momentum balance for the stack model

Given the gas composition as a function of space variable, the only unknown in Eq. (4) is temperature within the fuel cell. Differential heat balance equations are to be established for two gas phases (anode and cathode) and two solid phases (separator and cell layer), and they are generally expressed in the same form of the below equation.

$$\frac{\partial \rho u_x C_p T}{\partial x} + \frac{\partial \rho u_y C_p T}{\partial y} = \frac{\partial}{\partial x}\left(k\frac{\partial T}{\partial x}\right) + \frac{\partial}{\partial y}\left(k\frac{\partial T}{\partial y}\right) + \sum Q \quad (25)$$

When a stack is made up of n cells, $(n-1)$ bipolar separator plates and two end plates (upper and lower) are required. As a result, the total number of heat balance equations needed for a stack is $4n+1$ where $2n$ equations are for gas phases and $2n+1$ equations are for solid phases. For the solid phase, convection heat transfer terms are omitted, while the heat source term applies only to the cell layer. For the gas phase equation, axial and transverse velocities (u_x and u_y) are needed for the heat convection terms. In fuel cells, total molar flow rates change from inlet to outlet as Eqs. (22) and (23) indicate. Mass or volumetric flow rates should change too, and so do linear velocities. The change of linear velocities is taken into account by solving

Table 1
Specification of the MCFC stack model and parameters

Variable	Specification
Cell size	41 cm (L) × 76 cm (W) (approx. 3000 cm^2)
Number of cells	20
End separator plate thickness	80 mm
Bipolar separator plate thickness	5 mm
Instrumentation separator thickness	10 mm (with thermocouples inside)
Cell thickness	2.5 mm (anode + matrix + cathode)
Gas channel depth	0.8 mm
Gas channel flow porosity	0.3 (70% blockage of channel cross-section)
Fuel consumption to the feed	40% (anode utilization: 0.4)
Oxygen consumption to the feed	40% (cathode utilization: 0.4)
Current density	100 mA/cm^2
Gas flow configuration	Co-flow type
Fuel gas composition	H_2:CO_2:H_2O = 72:18:10
Oxidant gas composition	Air:CO_2 = 70:30 (O_2:N_2:CO_2 = 15:55:30)
Inlet gas temperature	550 °C
Anode inlet gas velocity	2.077 m/s
Cathode inlet gas velocity	4.984 m/s
Upper/lower end heating temperature	650 °C
Operating pressure	1 atm
Thermal conductivity of separator plates	25 W/m K
Thermal conductivity of cell layers	9.0 W/m K
Emissivity from separator plate	0.286
Emissivity from cathode layer	0.118
Emissivity from anode layer	0.586

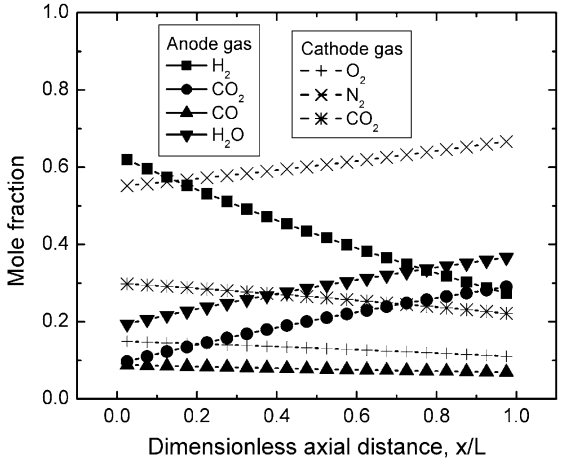

Fig. 2. Gas concentration profiles in the axial direction, from the assumption of uniform current density at 100 mA/cm^2 (after 10% conversion of the feed H_2 and CO_2 via the water-gas-shift reaction).

momentum balance equations. The total number of equations increases by including the momentum equations than solving the heat equations only.

$$\frac{\partial \rho u_x}{\partial x} + \frac{\partial \rho u_y}{\partial y} = \pm m_{CO_3^{2-}} \tag{26}$$

$$\frac{\partial \rho u_x u_x}{\partial x} + \frac{\partial \rho u_y u_x}{\partial y} = -\frac{\partial P}{\partial x} + \frac{\partial}{\partial x}\left(\mu \frac{\partial u_x}{\partial x}\right) + \frac{\partial}{\partial y}\left(\mu \frac{\partial u_x}{\partial y}\right) \tag{27}$$

$$\frac{\partial \rho u_x u_y}{\partial x} + \frac{\partial \rho u_y u_y}{\partial y} = -\frac{\partial P}{\partial y} + \frac{\partial}{\partial x}\left(\mu \frac{\partial u_y}{\partial x}\right) + \frac{\partial}{\partial y}\left(\mu \frac{\partial u_y}{\partial y}\right) \tag{28}$$

Heat transfer by thermal radiation (Q_{rad}) has been considered in some models known before [6–8], though it was not justified whether it has a significant effect on overall heat transfer in fuel cell stacks.

$$Q_{rad} = \frac{\sigma_B A_{cell}(T_{cell}^4 - T_s^4)}{1/\varepsilon_{cell} + 1/\varepsilon_s - 1} \tag{29}$$

where σ_B is the Stefan–Boltzmann constant and A_{cell} the surface area of electrodes. T_{cell}, T_s, ε_{cell}, and ε_s denote cell temperature, separator temperature, emissivities from cell and separator plates, respectively.

2.5. Thermal and fluid properties

The heat balance equations for the solid phase require thermal conductivity of separator plates and cell layers. As separator plates are made of stainless steel for which property data are known quite well, there is no problem to estimate thermal conductivity of separator plates. For the MCFC cell layer which is composed of anode (Ni-alloy), cathode (nickel oxide), electrolyte (molten carbonate salts), and porous ceramic matrix (alumina), on the other hand, it is difficult to estimate its effective thermal conductivity at the operating condition. A set of data we can search from literature is shown in Table 1.

Thermal and transport properties of gases can be estimated based on thermodynamic equations of an ideal gas state. Gas properties required in the fuel cell stack model are density (ρ), specific heat capacity (C_p), viscosity (μ), and thermal conductivity (k). The pure gas properties are all functions of temperature, and they are available from literature or estimated from well-known correlation equations [9,10].

$$\rho = \frac{PM}{RT} \tag{30}$$

$$C_p = a + bT + cT^2 \tag{31}$$

$$\mu = 26.69\frac{\sqrt{MT}}{\sigma^2}\left(\frac{1.16145}{(T^*)^{0.14874}} + \frac{0.52487}{\exp(0.7732T^*)} + \frac{2.16178}{\exp(2.43787T^*)}\right)^{-1} \tag{32}$$

with

$$T^* = \frac{k_B T}{\varepsilon}$$

$$k = \frac{\mu}{M}(2.25R + C_v) = \frac{\mu}{M}(1.25R + C_p) \tag{33}$$

The property of gas mixtures can also be estimated from correlation as a function of pure gas properties and gas composition [10,11].

$$\rho_{mix} = \frac{P}{RT}\left(\sum_j y_j M_j\right) \tag{34}$$

$$C_{p,mix} = \sum_j y_j C_{p,j} \tag{35}$$

$$\mu_{mix} = \sum_{i=1}^{n} \frac{y_i \mu_i}{\sum_{j=1}^{n} y_j \phi_{ij}} \tag{36}$$

$$k_{mix} = \sum_{i=1}^{n} \frac{y_i k_i}{\sum_{j=1}^{n} y_j \phi_{ij}} \tag{37}$$

where ϕ_{ij} is the binary interaction parameter between species i and j calculated from

$$\phi_{ij} = \frac{[1 + (\mu_i/\mu_j)^{0.5}(M_j/M_i)^{0.25}]^2}{[8(1 + M_i/M_j)]^{0.5}} \tag{38}$$

Some intrinsic gas parameters in the above correlation equations are listed in Table 2.

Table 2
Intrinsic parameters for calculation of MCFC gas properties

Species	M (g/mol)	$C_p = a + bT + cT^2$ (J/mol K)			Lennard-Jones parameter	
		a	b	c	σ (Å)	ε/k_B (K)
H_2	2	28.949	-5.855×10^{-4}	1.890×10^{-6}	2.827	59.7
CO_2	44	25.977	4.360×10^{-2}	-1.494×10^{-5}	3.941	195.2
CO	28	26.875	6.940×10^{-3}	-8.212×10^{-7}	3.690	91.7
H_2O	18	30.407	9.540×10^{-3}	1.183×10^{-6}	2.641	809.1
O_2	32	25.749	1.294×10^{-2}	-3.853×10^{-6}	3.467	106.7
N_2	28	27.313	5.190×10^{-3}	-7.212×10^{-10}	3.798	71.4

3. Numerical analysis of the fuel cell stack model

3.1. Model domain

The model considered for this study is a 20-cell stack with 3000 cm^2 cell area. Two end plates and 19 bipolar separator plates are needed for this 20-cell stack. Among the 19 bipolar plates, three are instrumentation plates that are thicker than other 16 plates as specified in Table 1. The instrumentation plates have thermocouples inside for temperature measurement. The measured temperature data was compared with predicted temperature curves, proving the validity of this MCFC stack model [12].

The model domain is divided into lots of rectangles, and thus the mathematical model equations are developed in a Cartesian coordinate system. Computational grids are created by number of grids in the *x*-direction for cell length and in the *y*-direction for cell layer, gas channel, and separator plates, respectively. Since the dimension of gas channel depth is very small (0.8 mm), even a single computational element for the channel depth creates a relatively very stiff ratio of Δx to Δy when Δx and Δy refer to the size of a computational grid element. The effect of grid numbers or sizes will be explained based on numerical computation results in the next section.

3.2. Numerical computation of the model equations

The heat and momentum balance equations were solved numerically using a computational fluid dynamics (CFDs) code. Among many CFD codes available these days, we selected PHOENICS (v2.2) for computation of the fuel cell stack model. This commercial code consists of the main solver (called EARTH) and many subroutines. One of the subroutine codes (called GROUND.FOR) is specifically made for users to implement their own equations. The fuel cell reaction and many correlation equations for electrode polarization and gas properties were implemented in this subroutine. The numerical computation procedure is based on the finite volume analysis method [13]. Equations for temperature are solved for values of grid centers and equations for gas flow fields are solved for face values of each grid using the SIMPLER algorithm.

The gas flow porosity in Table 1 indicates a partial blockage of gas channels, and it was set 0.3 to account for a significant effect of gas channel geometry on pressure drop which we observed during the operation test of the stack. The pressure drop may also be calculated in a different way using a friction loss coefficient [14].

Convergence of numerical calculation was judged by the whole field residuals that reflect the total sum of imbalances or errors of the solved—for variables in the finite volume equations during the solution procedure where the aim of the iteration process is to lower these errors as much as possible [15]. The residuals of pressure and velocity after convergence were much lower than normal values of these variables (0–10^4 N/m^2 and 0.1–5.0 m/s, respectively) by an order of 10^{-4}. The residual of temperature, on the other hand, was lower than a typical value (800–1000 K) by an order of 10^{-2}. Such a relatively high residual for temperature indicates that the computation of a temperature field is the toughest in this numerical calculation probably due to the multi-layer structure of cells and tiny thickness of cell components. A typical single run of numerical computation took about 30 min on a 650 MHz PC for 21 × 173 grids.

3.3. Boundary and source terms

Temperature at the stack boundary was expressed with a heat flux equation. The boundary heat flux equation requires surrounding temperature (T_0) as well as the stack boundary temperature.

$$q_{x\text{-boundary}} = -k\frac{\mathrm{d}T}{\mathrm{d}x} = k\frac{(T_{x\text{-boundary}} - T_0)}{\Delta x} \quad \text{(at inlet and outlet)} \tag{39}$$

$$q_{y\text{-boundary}} = -k\frac{\mathrm{d}T}{\mathrm{d}y} = k\frac{(T_{y\text{-boundary}} - T_0)}{\Delta y} \quad \text{(at upper/lower ends)} \tag{40}$$

At the upper and lower ends, surrounding temperature is the heating temperature (650 °C). The inlet is relatively cold since feed gas streams enter the stack usually at a lower temperature than the heating temperature. The inlet surrounding temperature will therefore approximate the inlet gas temperature. The outlet surrounding temperature is hardly predictable. We guessed it the same as that of the heating temperature, and this approximation turns out to be accurate when compared to measured data [12]. The characteristic length for boundary heat flux (Δx or Δy) is a parameter to be determined from details of stack design specifications.

Boundary conditions for the momentum equations are simple. The inlet gas condition is given from the operating condition (Table 1). The outlet gas follows the natural boundary condition with no pressure gradient. Reynolds number for fuel cell operation is within the laminar flow regime.

The differential equations are integrated over the finite volume of computational elements, resulting in a set of linear algebraic equations. Non-linear reaction or heat generation rates are represented in those algebraic equations as source/sink terms from the result of linearization. The linear coefficients may include dependency of temperature and/or partial pressures.

$$\phi_{\text{source}} = a - b\phi(x, y) = \phi_{\text{coe}}[\phi(x, y) - \phi_{\text{val}}] \tag{41}$$

where the rate of generation or consumption (ϕ_{source}) is expressed with a linearized coefficient (ϕ_{coe}) and a value (ϕ_{val}) for each dependent variable, $\phi(x, y)$. Non-linear terms, if there are any, are all incorporated into ϕ_{coe} and/or ϕ_{val}.

In the MCFC stack model, the source/sink terms are originated mostly from the cell reactions in electrodes. The cell

reactions are a crucial source of mass and heat in the fuel cell modeling and numerical simulations. Mass change in each gas phase affects more or less temperature and flow field calculation. In this study, we considered the effect of mass change by incorporating them in the overall mass continuity (Eq. (26)). In the computation code, it was implemented in the form of aforementioned linearized mass source at anode and sink at cathode on the surface of each cell layer. The heat of cell reactions was similarly treated as a linearized source term of the heat balance equation, and it was also implemented in the subprogram for temperature and concentration dependency of the linear coefficients.

4. Results and discussion

4.1. Effect of grid setting

We tried numerical computation with different sets of grid numbers for the identical stack specification. The four different settings we compared are listed in Table 3. The cell length (41 cm) was divided into 21 or 41 computational elements. The thickness of each cell layer was divided into three or five elements. The thickness of separator plates was divided into 3–9 elements. The depth of each gas channel was divided into 1–5 elements. The four different grid settings in Table 3 applied to the model and the results are compared in Fig. 3. Fig. 3(a) shows the shape of axial velocity profiles across the channel depth computed from the model for the four cases of Table 3. In Case I with a single computational element for gas channel depth, the axial velocity (u_x) profile along the y-direction is considered uniform (plug flow) as the velocity is represented by only a single value for the channel depth. In other cases (II–IV) where three of five elements were used for the same gas channel depth, a typical parabolic velocity profile is observed. The difference in velocity profile between a single and multiple elements certainly affects the calculated pressure drop from inlet to outlet shown in Fig. 3(b). Both cathode and anode gas pressure drop is significantly lower in Case I than those in the other cases. When the gas channel depth is divided into five elements (Case IV), the calculated pressure drop is a little higher than the cases of three elements (Cases II and III). Obviously, the number of computational element for gas channel depth influences flow field calculation in terms of pressure drop. With smaller number of computational elements, pressure drop is underestimated especially when a single element is used. This is probably due to the effect of viscous shear stress on channel wall which is not taken into account when the velocity profile is flat.

In contrast, the shape of temperature profiles is not much influenced by the number of computational grids as shown in Fig. 3(c). No matter how many grids are set for gas channel depth, vertical temperature profiles are uniform for the gas channel. Temperature prediction seems to be affected rather by the axial number of elements. Increasing the number of axial elements from 21 (Cases I and II) to 41 (Cases III and IV) results in a little increase of temperature by 3–4°.

We conclude that the number of computational grids for gas channel depth affects numerical calculation of gas flow fields but not temperature fields. As long as the purpose of numerical calculation is prediction of temperature fields only, a single computational element would suffice for each gas channel depth. As fuel cell stacks consist of lots of cells (usually several tens), reducing the number of computational grids for each layer speeds up the whole computation time greatly. If the purpose of analysis is to calculate pressure drop of gas streams, however, the gas channel depth should be divided into multiple grids for numerical accuracy.

4.2. Two-dimensional temperature distribution

A typical temperature field is shown in Fig. 4(a). The contour lines show how temperature is distributed by the heat released during fuel cell stack operation. The contour lines are not smooth, and this is because of abrupt change of temperature at the interface between many different gas and solid layers having different heat capacity and thermal conductivity. Temperature near the upper and lower end plates is close to the heating value (650 °C), and in most other region temperature contour lines appear to propagate from inlet to outlet. Temperature near the inlet is also close to the feed gas temperature, and temperature near the outlet is much higher. The feed gas enters the stack at 550 °C and exits at approximately 700 °C. This increase of gas temperature is caused by the heat generated from cells that is partly absorbed by gas streams and partly transferred between cells and separator plates. Therefore the exit temperature

Table 3
Four cases with different numbers of grid elements for numerical computation of the two-dimensional MCFC stack model

Number of computational elements	Case I	Case II	Case III	Case IV
Axial distance (cell length)	21	21	41	41
Upper/lower end plates	5	7	7	9
Instrumentation plates	5	5	5	7
Bipolar separator plates	3	3	3	5
Gas channel depth	1	3	3	5
Cell thickness	3	3	3	5
Total elements for 20 cells	21 × 173 (3633)	21 × 257 (5397)	41 × 257 (10537)	41 × 419 (17179)

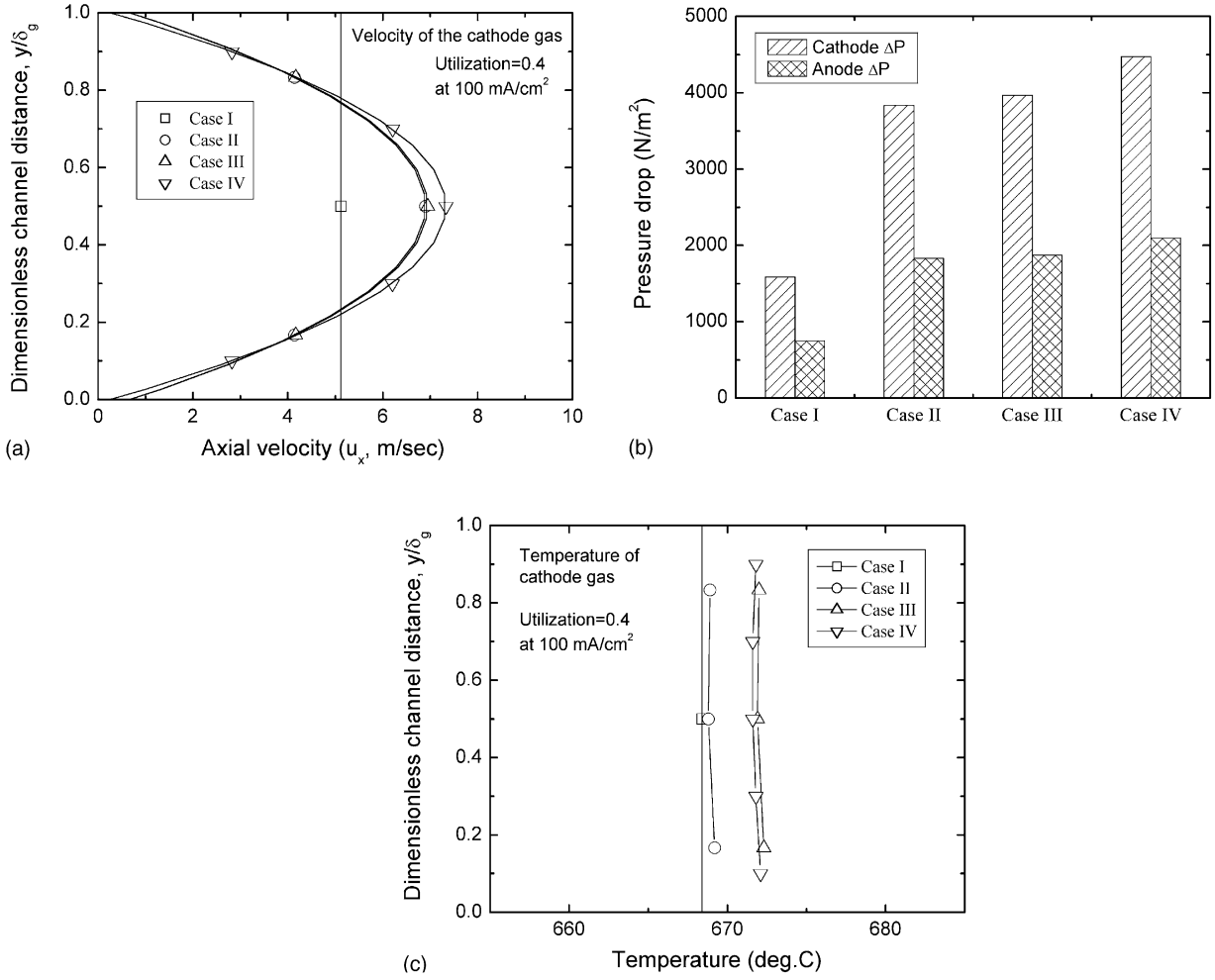

Fig. 3. Effect of grid setting (see Table 3) for gas channel depth: (a) velocity profile, $u_x(y)$; (b) pressure drop, $\Delta P = P_{\text{in}} - P_{\text{out}}$; (c) temperature profile, $T(y)$ at $x = \frac{1}{2}L$.

depends on the rate of cell reaction or current density. The temperature is also strongly influenced by gas utilization as it determines how much excess gas is introduced. These were studied earlier [1]. MCFC has a narrow operating temperature range (600–680 °C for stable long-run operation), compared to other types of fuel cells, mostly because of highly corrosive electrolyte. Keeping temperature within the range is important for MCFC, and this makes temperature prediction from the stack model very important.

As Fig. 4(a) shows, axial variation is most dramatic in this two-dimensional view of temperature distribution for the co-flow stack configuration. Especially the axial temperature curve at the center of stack height seems to represent the most significant characteristics of temperature change as the upper and lower regions are more influenced by external heating than the cell reaction. The axial temperature curves of anode and cathode gases are shown in Fig. 4(b) from inlet to outlet at several different cell locations. Cell #1 is the lowest one, and Cell #10 is at nearly the center of stack height. The axial temperature plots show almost an identical curve except at the lowest cell position. The maximum temperature is spotted a little before the stack outlet. This is reasonable since there is always heat loss from the stack to surroundings. The heat loss is accounted for in this model with the stack outlet boundary condition when stack temperature is very high and the surrounding temperature is set lower. The temperature curve near Cell #10 is the one we are going to benchmark in the remaining part of this paper.

4.3. Use of constant velocities

The momentum equations are required in the fuel cell stack model to calculate velocity fields and pressure drop of gas streams. They can also take the mass change of gas streams into consideration. Adding the momentum balance equation, however, makes the model more complicated and takes much longer computation time than solving the heat balance equation only. Linear velocities change within the cell not only because of change of temperature and gas composition but because of change of mass flux as already

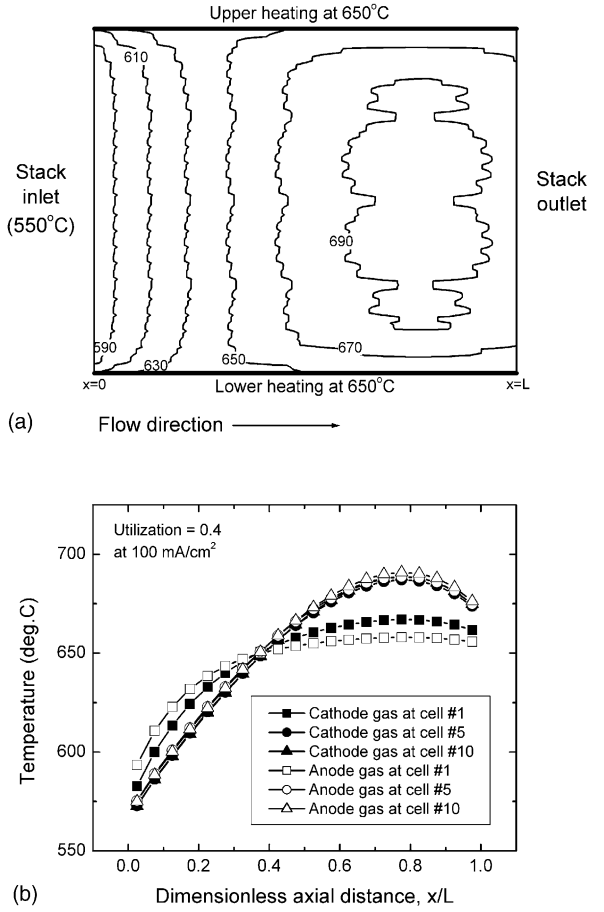

Fig. 4. A typical shape of temperature distribution in the co-flow MCFC stack: (a) temperature contours at the *x*–*y* cross-section; (b) axial temperature curves.

pointed out. If such a change of velocity has negligible effect on calculation of temperature field, the stack model can be solved using constant velocities without the momentum equations. In order to see whether we can use constant velocities, numerical calculation was done with only heat balance equations assuming velocities of gas streams are constant. Constant velocity values were estimated at the inlet condition (see Table 1). The resulted plot of Fig. 5, however, indicates the temperature calculated with constant velocities are not the same as that obtained by solving the momentum equations. The difference between the two temperature curves is 20–30 °C. Clearly, it is necessary to solve the momentum equations that accounts for the change of velocity. This also suggests the axial convection heat transfer term, which is related with gas velocity, is a determining factor of the overall heat transfer mechanism in fuel cells.

4.4. Effect of thermal radiation

Thermal radiation is a very complicated phenomenon. In some industrial processes, boilers in coal-fired power plants for example, it plays a key role in the overall heat transfer

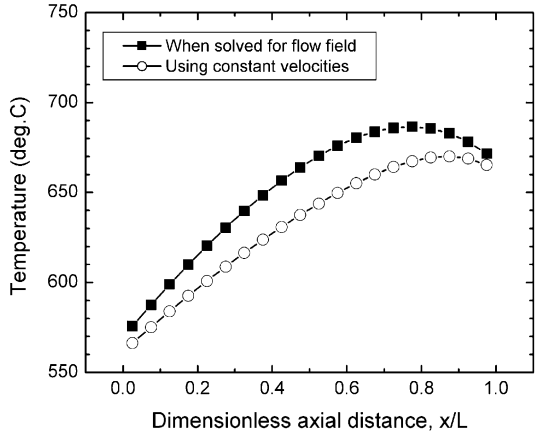

Fig. 5. Axial temperature curves with and without the momentum equations in the stack model.

mechanism. It has often been used in the fuel cell models, too, but, its influence on temperature calculation was not reported. Unlike heat conduction and convection terms, thermal radiation is not a built-in term in the heat balance equation (Eq. (25)). Therefore, thermal radiation is considered a heat source from cells and a heat sink into separator plates. The thermal radiation equation (Eq. (29)) should then be expressed in the form of linearized heat source/sink as in Eq. (41). In Fig. 6, axial temperature curves obtained from numerical calculation with and without the thermal radiation term are compared. The two temperature curves are almost identical, indicating the thermal radiation term can be ignored. This conclusion is not phenomenological, however, but is based on the simple thermal radiation model, Eq. (29), and the parameters we found from literature for SUS separator plates and cell components.

4.5. Effect of gas properties on temperature prediction

The temperature field of Fig. 4 was obtained with gas properties estimated from Eqs. (30)–(38) as functions of

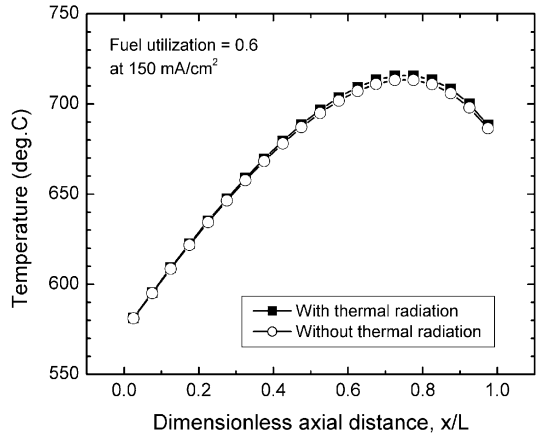

Fig. 6. Effect of thermal radiation on temperature prediction at 150 mA/cm^2.

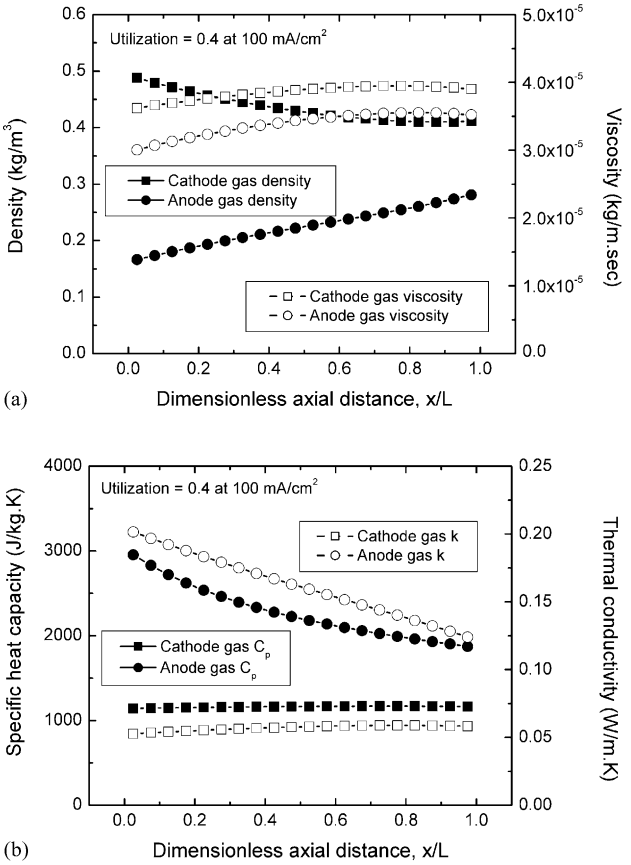

Fig. 7. Variation of gas properties in the axial direction: (a) density and viscosity; (b) specific heat capacity and thermal conductivity.

temperature and gas composition. The variation of those properties is plotted in Fig. 7. Fig. 7(a) shows the variation of two flow properties (density and viscosity), and Fig. 7(b) shows two thermal properties (heat capacity and conductivity). Cathode gas density decreases while anode gas density increases. Note that cathode gas loses CO_2 and O_2 from the cell reaction and anode gas gains H_2O and CO_2 in return for the loss of a much lighter gas species (H_2). As a result, the cathode gas becomes less denser as it flows from inlet to outlet, while the anode gas becomes much denser and heavier. Viscosity changes less than density as it is compared in Fig. 7(a). Both specific heat capacity and thermal conductivity decrease significantly from inlet to outlet for anode gas, but those two properties of cathode gas are almost constant from Fig. 7(b). Though the cathode gas loses some compounds, most of its composition is taken by nitrogen from air and therefore the change of composition in cathode gas is smaller than that in anode gas as shown in Fig. 2. Fig. 7(b) may therefore imply thermal properties are more influenced by gas composition than by temperature. In anode of which gas composition changes significantly, thermal properties change significantly as well. In cathode of which gas composition changes little due to excess nitrogen, thermal properties do not change significantly.

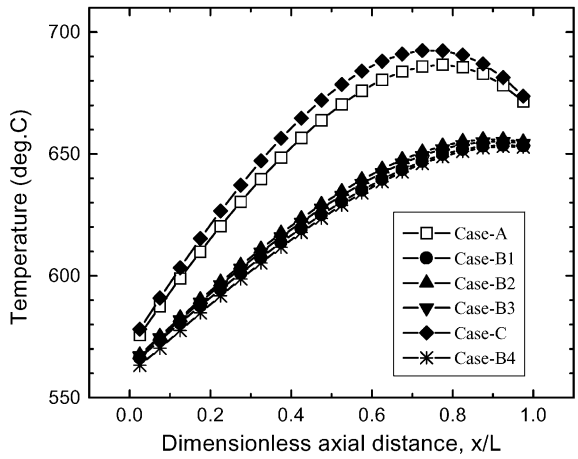

Fig. 8. Comparison of axial temperature curves with constant and non-constant gas properties (see Table 4).

When gas properties are estimated from the correlation equations as functions of temperature and gas composition, the fuel cell model has more non-linear equations solved together with the main equations and this makes numerical computation longer than using constant values for those properties. In fact, many fuel cell models use constant values for those gas properties. We conducted numerical calculation of the stack model with non-constant gas properties and constant gas properties. The constant property values were read from Fig. 7, and the calculated results are compared in Fig. 8. In Fig. 8, Case-A occurs when all the gas properties were estimated from the correlation equations and we will call this the standard case. Case-B1 occurs when gas properties were fixed at their inlet values. Case-B2 occurs when gas properties were fixed at their outlet values, and Case-B3 occurs when the average values between inlet and outlet properties were used. Case-C occurs when those gas properties were estimated from the correlation equations at a constant temperature (650 °C) to take into account the effect of gas composition only. These cases are tabulated to give a quick summary in Table 4. Fig. 8 indicates all the three cases (B1–B3) with constant gas properties result in an identical temperature curve which deviates from the temperature curve of the standard case (A). Obviously all or some gas properties should be estimated as functions of gas composition and temperature. The result of Case-C, on the other hand, is close to the standard case. Temperature-dependency of gas properties seems to be less significant than the influence of gas composition as we already noted.

When all constant properties were used together with constant gas velocities (Case-B4), the temperature curve is almost the same as that with non-constant gas velocities. We already figured the use of constant gas velocity influences temperature curve from Fig. 5, but the result of Fig. 8 indicates the effect of constant gas properties is more significant.

Now we know the calculation of temperature field is sensitive to variation of at least one or more gas properties. As

Table 4
Different sets of gas property estimation for numerical computation of the MCFC stack model

	Density	Specific heat capacity	Viscosity	Thermal conductivity
Case-A (standard)	$f(y_j, T)$	$f(y_j, T)$	$f(y_j, T)$	$f(y_j, T)$
Case-B1	Constant (inlet)	Constant (inlet)	Constant (inlet)	Constant (inlet)
Case-B2	Constant (outlet)	Constant (outlet)	Constant (outlet)	Constant (outlet)
Case-B3	Constant (average)	Constant (average)	Constant (average)	Constant (average)
Case-B4[a]	Constant (inlet)	Constant (inlet)	Constant (inlet)	Constant (inlet)
Case-C	$f(y_j)$ at 650 °C	$f(y_j)$ at 650 °C	$f(y_j)$ at 650 °C	$f(y_j)$ at 650 °C
Case-D1	$f(y_j, T)$	Constant (inlet)	Constant (inlet)	Constant (inlet)
Case-D2	Constant (inlet)	$f(y_j, T)$	Constant (inlet)	Constant (inlet)
Case-D3	Constant (inlet)	Constant (inlet)	$f(y_j, T)$	Constant (inlet)
Case-D4	Constant (inlet)	Constant (inlet)	Constant (inlet)	$f(y_j, T)$
Case-E1	Constant (inlet)	Anode: $f(y_j, T)$, cathode: constant	Constant (inlet)	Constant (inlet)
Case-E2	Constant (inlet)	Anode: constant, cathode: $f(y_j, T)$	Constant (inlet)	Constant (inlet)

[a] Case-B4 is when constant velocities were used.

listed in Table 4, we considered more cases with one of the gas properties being estimated from the correlation equations while the other properties are kept constant for their inlet values. Case-D1 occurs when only gas density was dependent on temperature and gas composition and the other three gas properties were constants. Case-D2 occurs when only specific heat capacity was dependent on temperature and gas composition, and so on. The results are compared in Fig. 9. The temperature curve of the standard case coincides with that of Case-D2 where specific heat capacity was estimated from the correlation equations. Temperature curves of the other three cases are almost identical, but significantly underestimate temperature by up to about 40 °C compared to that of the standard case. Apparently, calculation of temperature field is specifically influenced by specific heat capacity of gas streams. Specific heat capacity of gas streams should therefore be estimated as a function of gas temperature and composition, but the other gas properties can be treated constant in the stack model.

Specific heat capacity of cathode gas is in fact almost uniform from Fig. 7(b). It is therefore, probably anode gas specific heat capacity that delivers the sensitivity for temperature prediction. Numerical computation was done further with estimating only anode gas heat capacity from the correlation equations (Case-E1) and with estimating only cathode gas heat capacity from the correlation equations (Case-E2). In Fig. 10, the temperature curves of the standard case and of Case-D2 are compared to those of Cases-E1 and E2 where only either anode gas C_p or cathode gas C_p is estimated as a function of temperature and gas composition. As it shows, the temperature curve of Case-E2 occurs far below the standard temperature curve, indicating the estimation of only cathode gas C_p as a function of temperature and gas composition is not sufficient to predict the temperature curve we want to see. When only anode gas C_p is estimated as a function of temperature and gas composition, the temperature curve is close to the standard one. It is concluded that cathode gas heat capacity can also be treated a constant value. Only anode gas heat capacity should be estimated from the correlation equations so that it delivers the dependency of temperature prediction on the variation of gas composition.

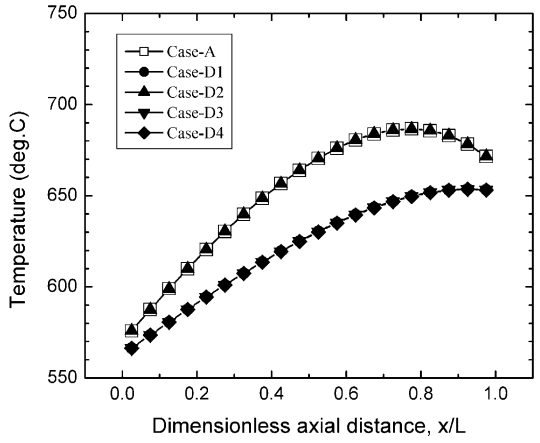

Fig. 9. Parametric analysis of axial temperature curves for dependency of gas property on temperature and gas composition (see Table 4).

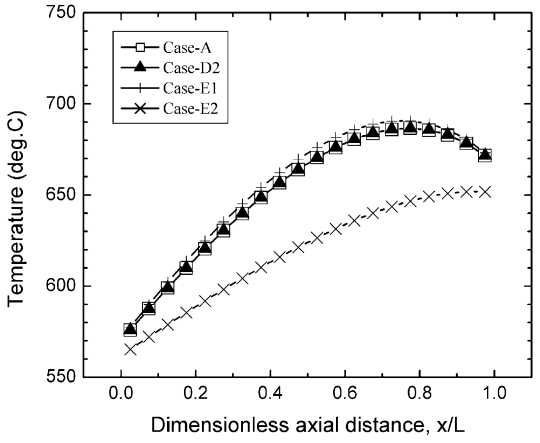

Fig. 10. Comparison of axial temperature curves with different estimation methods of gas heat capacities (see Table 4).

4.6. Convection heat transfer in fuel cells

The heat balance equation (Eq. (25)) in our stack model is expressed with convection, conduction, and heat source terms. The major heat source in fuel cell is cell layers where chemical energy in converted into electricity and heat. When there is no fuel reforming reactions in gas phase, no significant heat source or sink exists in the gas phase. Then the overall heat balance in the gas phase of fuel cell is represented with convection and interface transfer.

$$\rho u_x A_{\text{channel}} \theta C_p (\Delta T)_x = h A_{\text{cell}} (\Delta T)_y \quad (42)$$

where A_{channel} and A_{cell} are the gas channel cross-section area and the cell surface area, respectively, θ the porosity of gas channel and h is an interface heat transfer coefficient.

In our model, the interface heat transfer was treated with the concept of conjugate heat transfer [13,16]. A harmonic mean value of heat conductivity between two adjacent phases replaces the overall heat transfer coefficient (h) in such a case. In some other MCFC stack models, the interface heat flux was calculated with heat transfer coefficients which were estimated from the dimensionless heat transfer parameter (Nusselt number) with $Nu = 3$ [7,17] or $Nu = 3.77$ [18].

In high-temperature fuel cell stacks, temperature control or cooling is mostly done by heat convection in the gas flow direction, since an external cooling system is difficult to install. The most dominating heat transfer parameter would then be $\rho u_x C_p$ which has the same dimension as that of heat transfer coefficient (h, W/m^2 K). The values of $\rho u_x C_p$ for anode and cathode gas streams in Cases-A, D1–D4 are plotted in Fig. 11 in order to see why anode heat capacity should be estimated differently while others can be constant values. For anode gas, Case-E1 is equivalent to Case-D2, and Case-E2 is also equivalent to Case-D3 or D4. The figure shows the value of $\rho u_x C_p$ for anode gas is much higher when C_p is constant (D1–D4) than when C_p is estimated as a function of temperature and gas composition (A and D2). On the other hand, the value of $\rho u_x C_p$ for cathode gas is almost same no matter how C_p is estimated. This corresponds to the result from Figs. 9 and 10: temperature is predicted differently only when anode gas C_p is treated constant. This result confirms again the axial convection dominates the overall heat transfer in fuel cells, because we see a similarity between temperature curves and the variation of convection heat transfer rate represented by $\rho u_x C_p$.

Finally, we show axial variation of ρu_x (mass flux) and C_p independently to give a more clear explanation that convection heat transfer is dependent on temperature and composition for anode gas. We cannot separate ρ and u_x because mass flux is the conserved quantity from the overall mass continuity equation (Eq. (26)). When ρ changes, u_x changes in a way to make up for the change of ρ and keep a mass flux balance at any fixed position x. This is the reason why gas density has no influence on convection heat transfer and prediction of temperature curves. The mass flux itself, however, changes in the x-direction for both cathode and anode gas streams because of consumption and generation from the cell reactions. Fig. 12 shows the cathode mass flux decreases a little while the anode mass flux increases rapidly from inlet to outlet. The plots in Fig. 12 are made with relative values of mass flux and heat capacity to their inlet values so that we can compare them in a single plot. As in Fig. 7(b), the cathode gas heat capacity is almost constant even when it is calculated as a function of temperature and gas composition from the correlation equations. In anode, however, the constant C_p (Case-D1) and the non-constant C_p (Case-D2 or A) make some difference. Notice the anode C_p decreases in the axial direction when it is not constant. Let us consider the case that C_p is constant. If a constant value of anode gas heat capacity is used, the value of $\rho u_x C_p$ should be increasing more in the axial direction than the case when the non-constant C_p is used. This is Cases-D1, D3, D4, and Case-E2 for anode. The result is an overestimation of convection heat transfer rate by anode gas to cause the lower temperature curve as we saw from Figs. 9 and 10.

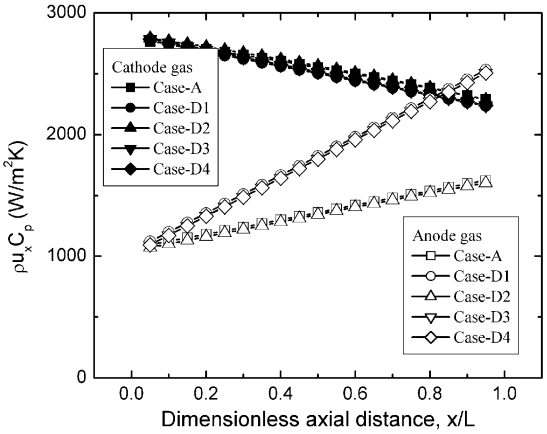

Fig. 11. Comparison of convection heat transfer by cathode and anode gas streams with constant and non-constant gas properties (see Table 4).

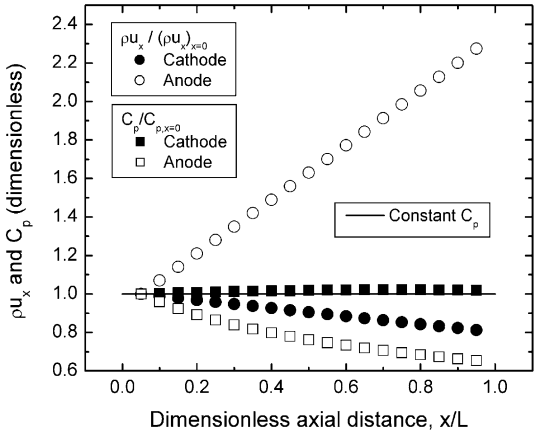

Fig. 12. Relative variation of mass flux and heat capacity of cathode and anode gas streams.

The reason for the identical temperature curves in Cases-A and D2 is because the convection heat transfer capacities of anode gas ($\rho u_x C_p$ values) are same as shown in Fig. 11. Fig. 11 indicates cathode gas has generally more heat convection capability than anode gas, but the gap is narrower near the outlet. If we ignore the dependency of anode gas C_p on gas composition, there is certainly a possibility of wrong estimation of temperature. Our conclusion will apply to MCFCs where anode gas has CO and CO_2. Other types such as PEM fuel cells which have different gas composition may have a different effect of gas properties on heat transfer. We will leave those for further study.

5. Conclusions

Several subjects regarding numerical analysis of a co-flow MCFC stack model were investigated. The subjects are grid number for channel depth, constant velocity, thermal radiation, and constant gas properties. All these are related to numerical accuracy of temperature prediction and computation time.

The effect of grid number for channel depth was studied because of tiny gas channel depth compared to relatively long gas flow length. The gas channel depth can be a single computational grid in the vertical coordinate without creating any significant errors on temperature calculation. However, a single grid for channel depth resulted in underestimated pressure drop compared to that of multiple grids. Therefore, a single grid of gas channel depth can be used only for the case of temperature prediction.

Convection heat transfer is undoubtedly the most dominating factor for the overall heat transfer mechanism in high-temperature fuel cells. Without the momentum equations, temperature is not predicted accurately because constant velocities do not account for the change of mass flux that influences convection heat transfer. Our result indicates that the thermal radiation is not necessary in the heat balance model of fuel cells.

In high-temperature fuel cells, temperature is controlled with the high flow-rate cathode gas. Due to the excess amount of nitrogen, the cathode gas has only a little variation of gas composition in the flow direction. This allows the use of constant gas property parameters for cathode gas in the stack model. The use of constant property parameters for anode gas is acceptable too, unless it overestimates the rate of heat convection by anode gas. The only occurrence of overestimated anode convection is when anode gas heat capacity is constant. We recommend therefore that anode gas heat capacity should be estimated as a function of gas composition and temperature using appropriate correlation equations.

Acknowledgements

This work was supported by Korea Electric Power Corporation (Grant 00ES02), R&D Management Center for Energy and Resources of The Korea Energy Management Corporation, and Korea Science and Engineering Foundation (Grant 1999-2-301-001-3).

References

[1] J.-H. Koh, B.-S. Kang, H.C. Lim, Effect of various stack parameters on temperature rise in molten carbonate fuel cell stack operation, J. Power Sources 91 (2000) 161–171.
[2] S. Sriramulu, P. Moore, P. Onnerud, J. Thijssen, Grove^{TM}: a fuel cell stack performance model, in: Fuel Cell Seminar, Portland, OR, 2000.
[3] H. Hirata, M. Hori, Gas-flow uniformity and cell performance in a molten carbonate fuel cell stack, J. Power Sources 63 (1996) 115–120.
[4] G. Wilemski, Simple porous electrode models for molten carbonate fuel cells, J. Electrochem. Soc. 130 (1983) 117–121.
[5] C.Y. Yuh, J.R. Selman, The polarization of molten carbonate fuel cell electrodes. 1. Analysis of steady-state polarization data, J. Electrochem. Soc. 138 (1991) 3642–3648.
[6] N. Zaima, Heat transfer characteristics in molten carbonate fuel cell, in: Electrochemical Society Proceedings of the Symposium on Fuel Cells, San Francisco, CA, 1989.
[7] T. Matsuyama, A. Matsunaga, T. Oagawa, Prediction of performance of molten carbonate fuel cell stack, in: Electrochemical Society Proceedings of the Fourth International Symposium on Carbonate Fuel Cell Technology, Montreal, Canada, 1997.
[8] F. Yoshiba, N. Ono, Y. Izaki, T. Watanabe, T. Abe, Numerical analysis of internal conditions of a molten carbonate fuel cell stack: comparison of stack performances for various gas flow types, J. Power Sources 71 (1998) 328–336.
[9] I. Barin, Thermochemical Data of Pure Substances, VCH Verlagsgesellschaft, Weinheim, Federal Republic of Germany, 1989.
[10] R.C. Reid, J.M. Prausnitz, T.K. Sherwood, The Properties of Gases and Liquids, 3rd Edition, McGraw-Hill, New York, 1977.
[11] J.M. Smith, H.C. Van Ness, Introduction to Chemical Engineering Thermodynamics, 3rd Edition, McGraw-Hill, New York, 1975.
[12] J.-H. Koh, B.-S. Kang, H.C. Lim, Analysis of temperature and pressure fields in molten carbonate fuel cell stacks, AIChE J. 47 (9) (2001) 1941–1956.
[13] S.V. Patankar, Numerical Heat Transfer and Fluid Flow, Hemisphere, New York, 1980.
[14] H. Hirata, T. Nakagaki, M. Hori, Effect of gas channel height on gas flow and gas diffusion in a molten carbonate fuel cell stack, J. Power Sources 83 (1999) 41–49.
[15] TR200, PHOENICS Reference Manual, CHAM Ltd., London, 1991.
[16] X. Chen, P. Han, A note on the solution of conjugate heat transfer problems using SIMPLE-like algorithms, Int. J. Heat Fluid Flow 21 (2000) 463–467.
[17] T.L. Wolf, G. Wilemski, Molten carbonate fuel cell performance model, J. Electrochem. Soc. 130 (1983) 48–55.
[18] N. Kobayashi, H. Fujimura, K. Ohtsuka, Heat and mass transfer in a molten carbonate fuel cell (experimental and analytical investigation of fuel cell temperature distribution), JSME Int. J. 32 (1989) 420–427.